Lipid Domain Structure Correlated with Membrane Protein Function in Placental Microvillus Vesicles†

Nicholas P. Illsley,* Herbert Y. Lin, and A. S. Verkman

Cardiovascular Research Institute, University of California, San Francisco, California 94143

Received July 9, 1986; Revised Manuscript Received September 26, 1986

ABSTRACT: Membrane fluidity properties of placental microvillus membrane vesicles (MVV) were determined from fluorescence anisotropy (r), dynamic depolarization, and lifetime heterogeneity studies of diphenylhexatriene (DPH), trimethylamino-DPH (TMA-DPH), and *cis*- and *trans*-parinaric acids (*c*-PnA and *t*-PnA). Plots of r against temperature for DPH and TMA-DPH in MVV had slope discontinuities at 26 °C (T_c, transition temperature); however, analysis of r in terms of probe rotational rate (R), limiting anisotropy (r_∞), and lifetime (τ) revealed that DPH reported a phase transition because of changes in r_∞, whereas the phase transition observed by TMA-DPH occurred primarily because of changes in R. Heterogeneity analysis using phase and modulation lifetimes at three frequencies showed that DPH and TMA-DPH lifetimes were homogeneous in MVV. Both long (>25 ns) and short (<6 ns) lifetime components were detected for *c*-PnA and *t*-PnA in MVV, corresponding to the probes in solid and fluid lipid phases. The fractional amplitude of the long lifetimes (solid phase) decreased from 0.86 to 0.12 with increasing temperature (5–55 °C) as the membrane passed through the phase transition, with 50% of the change occurring at 27 °C (*c*-PnA) or 33 °C (*t*-PnA). The activation energies for alkaline phosphatase, aminopeptidase M, and sodium–proton antiporter activities all showed discontinuities in the temperature range 27–31 °C. These results indicate (1) time-resolved fluorescence measurements are required to interpret correctly changes in steady-state anisotropy with temperature, (2) both solid and fluid lipid phases coexist in the MVV membrane over a broad temperature range centered around the phase transition temperature, and (3) membrane fluidity has an important modulating influence on microvillus membrane enzyme and transport functions.

The placental brush border and basolateral membranes form the interface between mother and fetus. They contain transport mechanisms for substrates, ions, vitamins, and other substances necessary for fetal growth and development. Prior studies in this laboratory have suggested that water transport across the brush border (microvillus membrane) may be modulated by the lipid phase state (Illsley & Verkman, 1986a); however, little is known about the physical structure of these key membrane barriers. In other membranes, including epithelial membranes, it has been established that changes in the physical state of the lipids influence membrane activities, both protein and non-protein mediated, particularly transmembrane transport activities (Houslay et al., 1980; Kutchai et al., 1980; Livingstone & Schachter, 1980; Yuli et al., 1981; Brasitus & Dudeja, 1985; Ives & Verkman, 1985; Worman et al., 1986; Verkman & Ives, 1986). The link between membrane enzymic or transport activities and the lipid state has not been resolved, due in part to the difficulties in defining and measuring accurately lipid states in natural membranes which contain large quantities of heterogeneous proteins and cholesterol.

In this paper, we examine how the physical state of membrane phospholipids in the placental brush border membrane modulates the activities of membrane-associated enzyme and transport functions. Steady-state anisotropy, dynamic depolarization, and lifetime heterogeneity analyses for a series of fluidity-sensitive fluorophores, including 1,6-diphenylhexa-1,3,5-triene (DPH),[1] TMA-DPH, *c*-PnA, and *t*-PnA, are used to characterize the temperature-dependent fluidity properties of the membrane. A well-defined thermotropic phase transition centered at 26 °C is shown to be present, which is associated with a marked decrease in the ratio of coexisting solid to fluid-phase phospholipids between 25 and 35 °C. On the basis of comparisons between the results of fluorescence measurements and the activation energies for a series of membrane-associated protein activities, the concept emerges that the fluidity state of the membrane phospholipids has an essential role in the modulation of membrane function.

Materials and Methods

Materials. DPH, TMA-DPH, *t*-PnA, and *c*-PnA were obtained from Molecular Probes (Junction City, OR). All other reagents were obtained from Sigma Chemical Co. (St. Louis, MO).

Vesicle Preparation. Placental microvillus vesicles were prepared from term (38–41 week) human placenta as described by Illsley and Verkman (1986a). The vesicle preparation was enriched ~24-fold in alkaline phosphatase (a microvillus membrane marker) compared to homogenate, while (Na^+/K^+)-ATPase activity (a basolateral membrane marker) was reduced ~3-fold compared to homogenate. Vesicles were suspended in 250 mM sucrose and 10 mM HEPES/Tris, pH 7.0 (buffer A), and frozen at −70 °C. Small

† This work was supported by NIH Grant AM35124 and by grants from the U.C.S.F. Academic Senate and MSC Clough Fund and from the HEDCO Foundation. N.P.I. was supported by NIH Training Grant AM07219.

* Address correspondence to this author.

[1] Abbreviations: DPH, 1,6-diphenylhexa-1,3,5-triene; TMA-DPH, 1-[4-(trimethylamino)phenyl]-6-phenylhexa-1,3,5-triene; *c*-PnA, *cis*-parinaric acid; *t*-PnA, *trans*-parinaric acid; MVV, microvillus vesicle(s); SUV, small unilamellar vesicle(s); NMG, *N*-methylglucamine; HEPES, *N*-(2-hydroxyethyl)piperazine-*N*′-2-ethanesulfonic acid; Tris, tris(hydroxymethyl)aminomethane; dimethyl-POPOP, 1,4-bis(4-methyl-5-phenyloxazol-2-yl)benzene.

0006-2960/87/0426-0446$01.50/0

unilamellar phosphatidylcholine vesicles were prepared immediately prior to use by sonication of egg lecithin phosphatidylcholine in buffer A (~25 mM) for 45 min at 4 °C under N_2 using a Microson MS-50 sonicator (Heat Systems-Ultrasonics, Farmingdale, NY). The vesicle suspension was centrifuged at 45000*g* for 30 min to remove titanium particles and lipid debris. The supernatant containing the SUV was removed and stored at 4 °C.

Assays. Alkaline phosphatase and aminopeptidase M were assayed by published methods (Livingstone & Schacter, 1980; George & Kenny, 1973) using 4-methylumbelliferyl phosphate and L-alanyl-4-methoxy-2-naphthylamide as substrates. In addition to measurement of enzyme activity in standard vesicle preparations, one vesicle preparation was incubated prior to the assay with 0.5% sodium deoxycholate to solubilize the alkaline phosphatase. This procedure left <10% of the alkaline phosphatase activity in the vesicle pellet after centrifugation at 450000*g* for 15 min, indicating a high degree of solubilization. The Na^+/H^+ exchange assay was performed by using the fluorescent pH indicator acridine orange. MVV were incubated for 16 h in 100 mM sucrose and 10 mM HEPES/Tris, pH 6.0, containing 50 mM potassium gluconate and 100 mM NMG/gluconate. Immediately prior to the assay, valinomycin (25 μg/mg of protein) was added to the MVV at a concentration which adequately clamped the membrane potential (Cabrini et al., 1986). MVV (0.2 mg of membrane protein/mL) were added to an assay buffer composed of 100 mM sucrose and 10 mM HEPES/Tris, pH 7.4, containing 50 mM potassium gluconate, 4 μM acridine orange, and either 100 mM NMG/gluconate or 100 mM sodium gluconate. Addition of MVV to the assay buffer caused rapid quenching of acridine orange fluorescence (<1 ns) as measured in an SLM 8225 fluorometer (SLM Instruments, Urbana, IL) using an excitation wavelength of 490 nm and an emission wavelength of 520 nm. The time course of fluorescence recovery was fitted to a single exponential, the exchange rate being calculated as the reciprocal of the exponential time constant and corrected for the non-Na^+-stimulated H^+ leak (Ives & Verkman, 1985). The identity of the antiporter was confirmed by demonstrating >95% inhibition of exchange activity by 0.2 mM amiloride in the presence of 25 mM Na^+.

Total phospholipid phosphorus was assayed by the method of Bartlett (1959) after extraction of membrane phospholipids by the method of Bligh Dyer (1959). Protein concentrations were determined by the method of Lowry et al. (1951). The lipid/protein ratio determined for MVV was 0.4 ± 0.1 μmol/mg of protein.

Fluorescent Probe Incorporation. Vesicles were diluted into N_2-gassed buffer A (MVV, ~0.1 mg/mL; SUV, ~250 μM), and fluorescent probes were added from stock solution in acetone (1–2 μL) to give a lipid/dye ratio greater than 400 (DPH and TMA-DPH) or 200 (*t*-PnA or *c*-PnA). The cuvettes were sealed under N_2, and vesicles were incubated in the dark at 23 °C for 60 min prior to measurement of fluorescence. Nonfluorescent reference samples were similarly prepared except that the aliquot of acetone added to the vesicles contained no probe. Stock solutions of DPH, TMA-DPH, *t*-PnA, and *c*-PnA were stored under N_2 at −20 °C in sealed, darkened vials.

Fluorescence Measurements. Measurements of fluorescence were made by using an SLM 4800 spectrofluorometer (SLM Instruments, Urbana, IL) equipped with a thermostated cuvette holder. Temperatures were measured with a thermistor (YSI R8415-30, Cole-Palmer, Chicago, IL) inserted into the cuvette, and all samples were equilibrated with respect to temperature prior to fluorescence measurement. Steady-state anisotropy (r) was measured by using the L format with background subtraction at an excitation wavelength of 310 nm (*t*-PnA and *c*-PnA) or by using the T format at 360 nm (DPH and TMA-DPH; excitation scattering <1%) with 4-nm band-pass. Emission light was filtered through high-pass 3-mm Schott glass-type GG 400 or 420 filters, respectively (Melles Griot, Irvine, CA; 50% transmittance of 405 or 425 nm). Depolarization due to scattering of emission light by vesicles was corrected by using an empirical relationship between anisotropy and sample absorbance similar to that described by Teale (1969) and Lentz et al. (1979): $\ln (r/r_z) = 1 - KA$ where r is the observed anisotropy, r_z is the anisotropy at zero dilution, A is the absorbance of the sample (in the absence of fluorophore), and K is a proportionality constant. K was determined for both excitation wavelengths from a linear regression of $\ln r$ on A for a series of six sample dilutions.

Fluorescence lifetimes were measured by the phase modulation method (Spencer & Weber, 1969; Weber, 1977) as described by Barrow and Lentz (1983, 1985). The excitation wavelength was 310 nm for *t*-PnA and *c*-PnA and 360 nm for DPH and TMA-DPH, using a 0.5-nm band-pass. Measurements were made with the excitation polarizer 35° from vertical and in the absence of an emission polarizer (Barrow & Lentz, 1985). Fluorescence emission was detected through 3-mm Schott glass-type GG 400 or GG 420 filters. The steady-state and dynamic photomultiplier zero-fluorescence offsets were adjusted to give zero intensity with the emission shutter closed. Fluorescence intensities of sample and reference were matched to within 4% for all lifetime measurements. The central peak obtained from the Debye–Sears modulation tank was used to minimize off-frequency Fourier components of the modulated light. On-line data acquisition and computation was performed with an IBM PC/XT, averaging five pairs of alternate sample and reference measurements.

Sample lifetimes were measured against isochronal reference standards (Barrow & Lentz, 1983, 1985). The isochronal standard used for DPH and TMA-DPH lifetimes was DPH in hexadecane, and for *t*-PnA and *c*-PnA, it was t-PnA in hexanol. The lifetimes of the isochronal standards were initially determined at 23 °C against the phase lifetimes of dimethyl-POPOP in absolute ethanol (1.45 ns; Lakowicz et al., 1981) at modulation frequencies of 6, 18, and 30 MHz. The temperature dependence of the isochronal standard was then determined by measuring its lifetime at various temperatures against an identical sample maintained at 23 °C. Phase (τ_p) and modulation (τ_m) lifetimes were calculated from eq 1 and 2 where ϕ_s and ϕ_r are the sample and reference phase angles,

$$\tau_p = \omega^{-1} \tan [\phi_s - \phi_r + \tan^{-1} (\omega\tau_r)] \quad (1)$$

$$\tau_m = \omega^{-1}[(1 + \omega^2\tau_r^2)/m^2 - 1] \quad (2)$$

m is the sample modulation factor, τ_r is the reference lifetime, and ω is the modulation frequency in radians per second.

Analysis of fluorescence lifetime data obtained at 6-, 18-, and 30-MHz modulation frequencies for ground-state heterogeneity was performed by using a modification of the χ^2 minimization procedure described by Barrow and Lentz (1983). χ^2 was calculated from the equation:

$$\chi^2 = \sum_{\omega}[(\tau_p - \tau_p^c)^2/\sigma_p^2 + (\tau_m - \tau_m^c)^2/\sigma_m^2] \quad (3)$$

where the summation is carried out over all modulation frequencies used. σ_p and σ_m are standard deviations for measured phase and modulation lifetimes at each frequency, and τ_p^c and τ_m^c are phase and modulation lifetimes calculated by using

the parameters being fitted including the lifetimes (τ_i) and fractional amplitudes (α_i) of the ith lifetime component. τ_p^c and τ_m^c were calculated by using the relations given by Weber (1981, eq 1–8). After selection of initial guesses for the fitted parameters, χ^2 was minimized by sequential gradient and grid search methods as described by Bevington (1969). The grid search was used after χ^2 changed by less than 1% (typically 3–6 iterations). The combination search method was found to be superior to either method alone as the gradient search was inaccurate and oscillated near the χ^2 minimum because of subtraction of nearly equal quantities, whereas the grid search, if used initially, converged very slowly and frequently to a local minimum.

Differential polarized phase fluorometry was used to determine the rotational rate (R) and limiting anisotropy (r_∞) of DPH and TMA-DPH by using the method described by Lakowicz et al. (1979) which is valid for isotropic rotations of a homogeneous hindered fluorophore. R and r_∞ for DPH and TMA-DPH in MVV were calculated from measurements of steady-state anisotropy (r), phase lifetime (τ_p), and differential tangent (tan Δ) measured at 18 mHz and r_0, the anisotropy in the absence of rotational motion. An r_0 value of 0.390 was used for both DPH and TMA-DPH (Lakowicz et al., 1979; Prendergast et al., 1981).

Results

Steady-State Anisotropies of DPH and TMA-DPH. The steady-state anisotropy of DPH was measured between 10 and 50 °C at 1 °C intervals. Anisotropy measurements were extrapolated to zero dilution to correct for emission scattering using a proportionality constant (K) of 0.23 ± 0.02 and the optical density of the sample (minus fluorophore) measured at 360 nm. The data for two samples, typical of four taken from separate placental preparations, are shown in Figure 1A. The experimental data were plotted as Δr against T^{-1} to visually offset data from separate samples. The curves were fitted to a double-connected straight line using a four-parameter, generalized Newton's least-squares fitting procedure in which the two slopes, breakpoint temperature (T_c), and intercept on the Δr axis were varied. Similar biphasic fits were found for the four separate preparations with a T_c of 25.8 ± 2.2 °C (mean ± SD). The mean slope above T_c (0.26 ± 0.02 K) was significantly higher ($p < 0.01$; Student's paired t test) than that below T_c (0.17 ± 0.02 K). The change in r was ~0.06 over the range 10–50 °C. The biphasic curve shape was suggestive of a membrane lipid-phase transition taking place at 26 °C.

The steady-state anisotropy of TMA-DPH was measured in an identical manner. Plots of Δr against T^{-1} for TMA-DPH are shown for two samples, typical of four, in Figure 1B. The data fitted biphasic curves with a mean T_c of 25.9 ± 2.5 °C and slopes of 0.12 ± 0.04 K above T_c and a significantly lower slope ($p < 0.05$) of 0.08 ± 0.02 K below T_c. In comparison to DPH, the change in r between 10 and 50 °C for TMA-DPH (~0.03) was approximately 50% lower; however, the biphasic curve shape suggests that TMA-DPH is also influenced by the postulated membrane phase transition.

Limiting Anisotropy and Rotational Rate. When the rotational motions of a fluorophore are hindered, fluorescence anisotropy does not decay to zero as described by the Perrin equation. Instead, a nonzero limiting anisotropy (r_∞) is observed at times which are long in comparison to the fluorescence lifetime (Weber, 1977). The rotational characteristics of an isotropic, hindered rotating fluorophore are described by two parameters: r_∞, which is related to the degree to which the angular range of motion (or rotational freedom) is hindered, and the rotational rate of the fluorophore (R). R and r_∞ were determined from r_0, r, τ, and tan Δ as described under Materials and Methods.

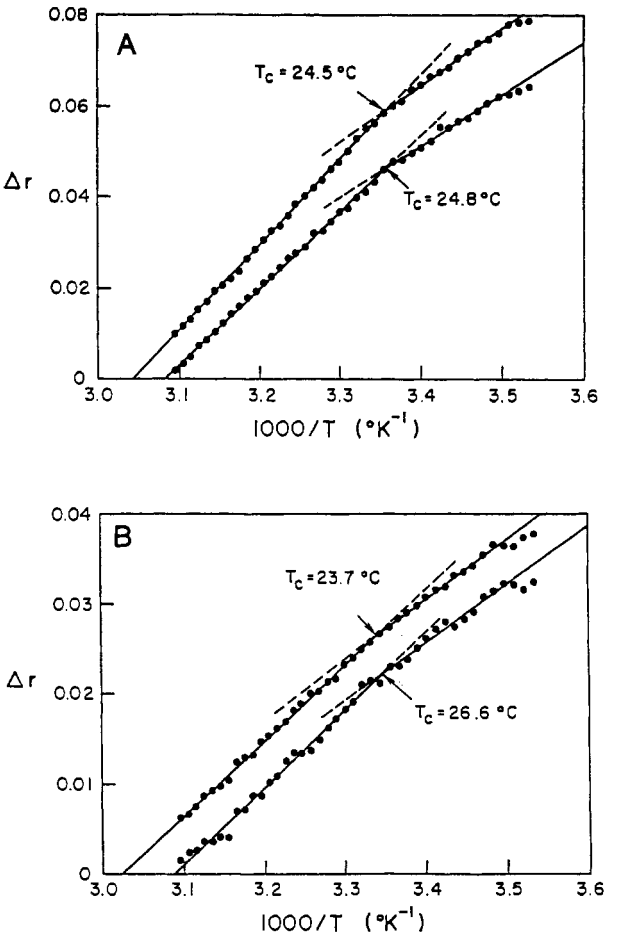

FIGURE 1: Temperature dependence of DPH and TMA-DPH steady-state anisotropy. Changes in Δr (r offset arbitrarily to separate data from individual experiments) with temperature for (A) DPH and (B) TMA-DPH in MVV. MVV (lipid/dye ~400; 0.1 mg of membrane protein/mL) sealed under N_2 and incubated with probe for 60 min in the dark at 23 °C prior to fluorescence measurement. Anisotropy measurements were corrected for emission scattering as described in the text. Standard deviations of the data were uniformly below 0.001 (0.5%) and therefore not plotted. Connected lines fitted to data by using a four-parameter, least-squares procedure for double, connected straight lines. For DPH (A), the absolute values of r at T_c were 0.2789 (upper curve) and 0.268 (lower curve). For TMA-DPH (B), the absolute values of r at T_c were 0.2971 (upper curve) and 0.2943 (lower curve).

tan Δ was measured for DPH in MVV at 18 MHz over the temperature range 14–50 °C (Figure 2A). tan Δ showed an increase in the range 20–30 °C, followed by a decrease in the region from 35 to 50 °C. This profile resembles a broadened version of the tan Δ profile observed for synthetic lipid bilayers, which shows a sharp increase at the phase transition followed by a slow decrease at temperatures above the phase transition (Lakowicz, 1979). tan Δ_{max}, calculated from r_o, τ_p, and ω, was 0.172. The tanget defect (tan Δ_{max} – tan Δ_{obsd}) was ~0.14 (80% of tan Δ_{max}), suggesting that DPH is a hindered rotator in placental microvillus membranes. The R values calculated for DPH in a single MVV preparation (typical of three) are shown in Figure 2B. Over the temperature range 10–50 °C, R increased from 0.14 ± 0.01 to 0.25 ± 0.01 radian/ns (mean ± SD; $n = 3$). The temperature dependence of r_∞ calculated for DPH in one placental preparation, typical of three, is shown in Figure 2C. In all cases, the data best fit to a biphasic curve resulting with a T_c of 23.7 ± 2.2 °C and significantly differing

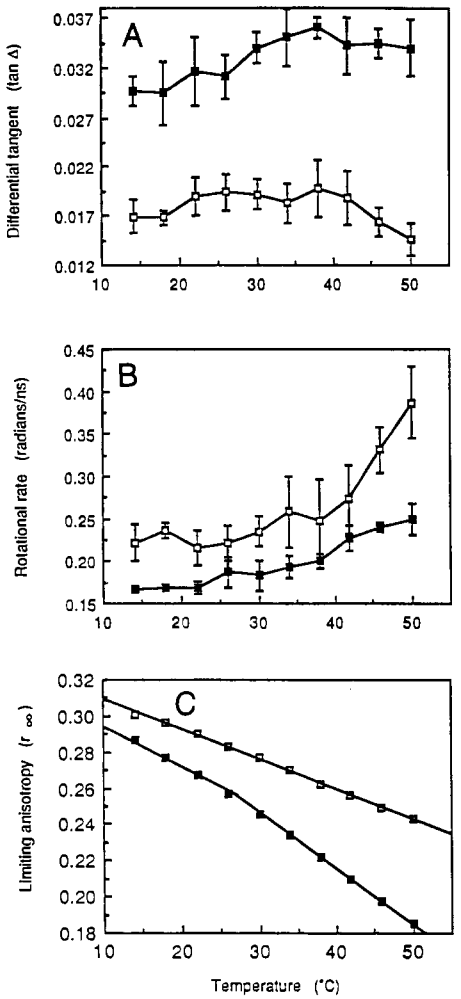

FIGURE 2: Anistropy decay measurements of DPH and TMA-DPH fluorescence. Temperature dependence of tan Δ (A), R (B), and r_∞ (C) for DPH (closed squares) and TMA-DPH (open squares). Samples were prepared as in Figure 1. tan Δ was measured at a modulation frequency of 18 MHz. R and r_∞ were calculated as described under Materials and Methods. Plots shown are typical of those from three separate placental preparations. Each tan Δ and R point is the mean (±SD) of six measurements. Standard deviations for r_∞ were under 0.007 and therefore not plotted.

curve slopes of (2.2 ± 0.3) × 10^{-3} °C^{-1} below and (2.7 ± 0.2) × 10^{-3} °C^{-1} above T_c ($p < 0.01$). Plots of r_∞ against r (not shown) were linear ($r_\infty = 1.008r - 0.014$), suggesting that the steady-state anisotropies were primarily measuring rotational freedom rather than rotational dynamics.

The data for TMA-DPH in MVV are also shown in Figure 2A–C. tan Δ showed a small increase at ~20 °C, followed by a decrease between 38 and 50 °C (Figure 2A). The tangent defect for TMA-DPH (0.112; 86% of tan Δ_{max}) was similar to that for DPH, suggesting that TMA-DPH rotation was also hindered. R values calculated for TMA-DPH were greater than those observed for DPH and showed an increase from 0.22 ± 0.01 to 0.40 ± 0.04 radian/ns ($n = 3$) between 14 and 50 °C (Figure 2B). Unlike DPH, r_∞ for TMA-DPH (Figure 2C) fitted to a straight line for all three sets of experimental data with a mean slope of (1.2 ± 0.3) × 10^{-3} °C^{-1} ($n = 3$). Plots of r_∞ against r were best fit to a straight line ($r_\infty = 1.021r - 0.016$).

Fluorescence Lifetimes of DPH and TMA-DPH. DPH and TMA-DPH lifetimes were measured relative to an isochronal standard, DPH in hexadecane. The lifetime of the isochronal standard was calibrated at 23 °C against dimethyl-POPOP in absolute ethanol. Phase lifetimes for 0.5 μM DPH in hexadecane were 9.75 ± 0.21, 9.71 ± 0.10, and 9.43 ± 0.28 ns at 6, 18, and 30 MHz, respectively. The temperature dependence data for the isochronal standard fitted to a straight line [τ_r (ns) = 10.05 − 0.017T; data not shown], and interpolated points were used for reference values.

Table I: DPH and TMA-DPH Fluorescence Lifetimes in Microvillus and Synthetic Lipid Vesicles[a]

probe	vesicles	T (°C)	τ_1 (ns)	α_1	τ_2 (ns)	α_2
DPH	SUV	15	8.59	0.98	0.29	0.02
		20	8.33	0.98	0.37	0.02
		25	8.11	0.98	0.44	0.02
		30	7.93	0.98	0.37	0.02
		35	7.63	0.98	0.32	0.02
		40	7.45	0.98	0.36	0.02
		45	7.22	0.98	0.51	0.02
DPH	MVV	15	9.96	0.98	0.23	0.02
		20	10.08	0.97	0.11	0.03
		25	9.96	0.98	0.23	0.02
		30	10.26	0.98	0.35	0.02
		35	10.32	0.98	0.35	0.02
		40	10.19	0.99	0.40	0.01
		45	10.16	0.99	0.37	0.01
TMA-DPH	MVV	15	7.36	0.99	0.20	0.01
		20	7.20	0.99	0.17	0.01
		25	7.09	0.98	0.19	0.02
		30	6.93	0.98	0.15	0.02
		35	6.87	0.96	0.16	0.04
		40	6.65	0.96	0.16	0.04
		45	6.48	0.95	0.20	0.05

[a] Lifetimes (τ_i) and fractional amplitudes (α_i) of the DPH and TMA-DPH lifetime components calculated by heterogeneity analysis as described under Materials and Methods.

DPH self-quenching and/or perturbation of the bilayer structure has been suggested to occur at low lipid/dye ratios in synthetic bilayer vesicles (Barrow & Lentz, 1985). DPH phase and modulation lifetimes were measured at three frequencies at lipid/dye (mol/mol) ratios of 20–1500. It was found that all lifetimes increased ~1 ns between lipid/dye ratios of 20/1 and 350/1 and then remained constant. Addition of the fluorophore solvent, acetone, had no effect on DPH lifetime.

DPH lifetime heterogeneity analysis was first performed on SUV, a single-phase membrane system. Phase and modulation lifetimes were measured at 6, 18, and 30 MHz relative to the isochronal DPH standard, between 15 and 45 °C. The heterogeneity analysis carried out on the SUV data (Table I, top section) demonstrates that 98% of the SUV fluorescence was attributable to a single-lifetime component. The lifetimes decreased with increasing temperature.

DPH and TMA-DPH lifetimes in MVV were also measured at 6, 18, and 30 MHz (Table I, bottom). The majority of DPH (>97%) and TMA-DPH (>95%) fluorescence was observed to be associated with a single lifetime; the second lifetime component (<1 ns) probably represents scattered light and is of the order of likely errors in lifetime estimation (Barrow & Lentz, 1985). DPH lifetimes showed no significant changes with temperature, but TMA-DPH lifetimes, like those of DPH in SUV, showed a decreasing trend with increasing temperatures.

Previous reports have raised the possibility of a DPH photodecomposition product contributing significant fluorescence, a phenomenon which might be increasingly important with continued exposure to light (Parasassi et al., 1984; Barrow & Lentz, 1985). We tested for this possibility by incubating two identical MVV/fluorophore samples (DPH and TMA-DPH) at 23 °C in the dark for 60 min. The first of each pair was used for a series of lifetime measurements at increasing tem-

peratures up to 50 °C, while the other remained in the dark, at 4 °C. After the lifetime of the first sample was measured at 50 °C, the second was rapidly warmed to 50 °C, and an identical lifetime measurement was performed. No significant difference was observed between the two samples for either DPH or TMA-DPH. This result combined with lack of a 3-ns lifetime (observed for DPH in the other reports and classified as a decomposition product) suggested that there were no fluorescent DPH derivatives present in our samples due to decomposition.

Fluorescent Lifetimes of t-PnA and c-PnA. The lifetimes of the parinaric acids are known to depend strongly on the physical state of their lipid environment. A long-lifetime component (>25 ns) has been demonstrated for both *t*-PnA and *c*-PnA in solid-phase lipids while a short-lifetime component (1–5 ns) is measured in the fluid phase of phospholipids (Wolber & Hudson, 1981). In addition, *t*-PnA partitions preferentially into solid-phase lipids (solid/fluid partition coefficient, $K_p^{s/f}$, of 3–5) while *c*-PnA partitions equally between solid and fluid phases ($K_p^{s/f}$ of 0.6–0.9; Sklar et al., 1979; Schroeder, 1983). We used the unique properties of these probes to examine the temperature dependence of domain behavior in MVV.

The lifetimes of *t*-PnA and *c*-PnA were measured relative to an isochronal standard, *t*-PnA in hexanol. The phase lifetimes of 2 μM *t*-PnA in hexanol were 1.64 ± 0.18, 1.68 ± 0.03, and 1.64 ± 0.03 ns at 6, 18, and 30 MHz, respectively, and were not significantly different from lifetimes of 5 μM *t*-PnA in hexanol. The temperature dependence of the isochronal standard was fitted to a straight line [τ_r (ns) = 2.51 − 0.035*T*], and interpolated values were used for the reference lifetimes.

Two short lifetimes were reported for *t*-PnA in fluid-phase lipids by Wolber and Hudson (1981) (6.8 and 3.1 ns at 23 °C). Our measurements of *t*-PnA lifetimes in SUV also revealed two short-lifetime components (6.3 and 0.85 ns at 23 °C) with fractional intensities of 0.84 and 0.16.

The phase and modulation lifetimes of *t*-PnA and *c*-PnA at 6, 18, and 30 MHz were measured at 5 °C intervals from 5 to 55 °C. Heterogeneity analysis performed on these data showed that, with the exception of the *t*-PnA measurements at 55 °C, the data for both *t*-PnA and *c*-PnA fitted well to a two-component model (three-parameter regression) with ground-state heterogeneity. A four-parameter regression which included a fractional amplitude for a zero-lifetime component (scattering) did not significantly improve the fit. The best fit for the *t*-PnA data at 55 °C included a zero-lifetime component with a fractional amplitude of 0.15. Figure 3A shows the lifetime of both components for *t*-PnA and *c*-PnA between 5 and 55 °C. With the exception of the measurements at 55 °C, the long-lifetime component (τ_1) of *t*-PnA was significantly greater than that for *c*-PnA at all temperatures. The short-lifetime components (τ_2) for *c*-PnA and *t*-PnA were similar at all temperatures. The fractional amplitudes (α_1) for the long-lifetime components of both *t*-PnA and *c*-PnA are plotted against temperature in Figure 3B. For both probes, α_1 decreased from >0.8 at 5 °C to <0.15 at 55 °C. The midpoint of the decrease in α_1 occurred at a lower temperature for *c*-PnA (~28 °C) than for *t*-PnA (~33 °C).

Steady-State Anisotropy of t-PnA and c-PnA. *r* was corrected to zero dilution for both probes by using a depolarization proportionality constant (*K*) of 0.116 ± 0.010 and the optical density of the sample (minus fluorophore) at 310 nm. The corrected anisotropies are shown plotted against temperature in Figure 3C. The ground-state heterogeneity demonstrated

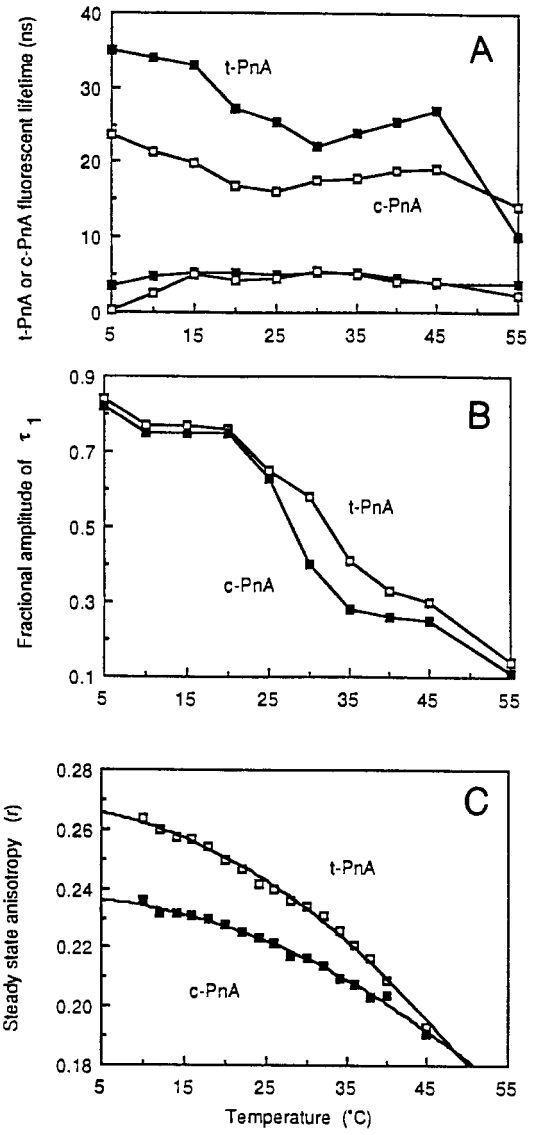

FIGURE 3: Fluorescent lifetimes, fractional amplitude of the solid-phase lifetime component, and steady-state anisotropy of *t*-PnA and *c*-PnA in MVV. MVV in N_2-gassed buffer A (~0.1 mg of membrane protein/mL) incubated for 60 min in the dark at room temperature with *t*-PnA or *c*-PnA at a lipid/dye ratio of 200, prior to measurement of fluorescence. Phase and modulation lifetime measurements performed at 6, 18, and 30 MHz using *t*-PnA in hexanol as the isochronal standard as described in the text. (A) Temperature dependence of *t*-PnA and *c*-PnA lifetimes calculated from heterogeneity analysis of lifetime data (see text for details of heterogeneity analysis). (B) Temperature dependence of the fractional amplitude of the *t*-PnA and *c*-PnA long- (solid phase) lifetime component calculated from heterogeneity analysis of sample data described above. (C) Temperature dependence of steady-state anisotropy for *t*-PnA and *c*-PnA, fitted to quadratic equations. Standard deviations for measurements of *r* less than 0.01 and consequently not plotted.

by both *t*-PnA and *c*-PnA in MVV (see previous section) precluded determination of r_∞ and *R* for these fluorophores.

Temperature Dependence of Membrane-Bound Enzyme Activities. Alkaline phosphatase activity was measured in MVV at temperatures from 15 to 45 °C by using a single-step assay which measured the cleavage of 4-methylumbelliferyl phosphate. Assays were initially performed at 15 and 45 °C in the presence of the normal (1 mM) and double substrate concentrations to determine whether the substrate concentration was saturating at both extremes of temperature (Silvius et al., 1978). No significant differences in enzyme activity were noted between the two substrate concentrations at either temperature. The Arrhenius plots of alkaline phosphatase

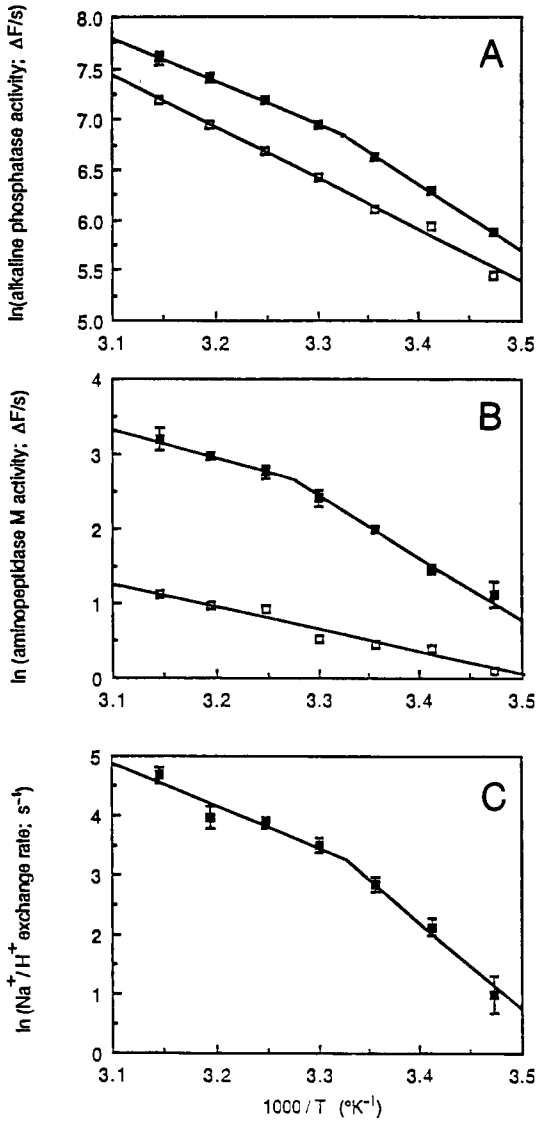

FIGURE 4: Temperature dependence of alkaline phosphatase, aminopeptidase M, and sodium/proton antiporter activities. Arrhenius plots of (A) alkaline phosphatase activity, (B) aminopeptidase M activity, measured both before (closed squares) and after deoxycholate solubilization (open squares), and (C) sodium/proton exchange activity. Each point represents the mean ± SD of three measurements, and the plots are typical of two (alkaline phosphatase) or three (aminopeptidase and Na^+/H^+ exchange) sets of measurements from separate placental preparations. The biphasic curves were fitted by a four-parameter, least-squares procedure for a double, connected straight line. Straight line fit by linear regression.

activity for one preparation typical of two are shown in Figure 4A. Plots from both preparations fitted to biphasic curves with slope discontinuities at 28.0 ± 1.3 and 28.4 ± 3.5 °C. The slopes at temperatures above T_c (−4.4 ± 0.2 K) were significantly less ($p < 0.01$) than those below T_c (−6.3 ± 0.1 K). The activity of the deoxycholate-treated enzyme was lower than that of the native enzyme and was found to fit best to a straight line with a slope intermediate to the slopes of the native enzyme above and below T_c.

Similar temperature-dependence experiments were carried out for aminopeptidase M using a single-step assay which measured the cleavage of L-alanyl-4-methoxy-2-naphthylamide. No significant differences were noted between normal (0.2 mM) and doubled substrate concentrations at either 15 or 45 °C. The Arrhenius plot of enzyme activity before and after deoxycholate treatment from one preparation (typical of three) is shown in Figure 4B. Aminopeptidase activity in the three preparations displayed biphasic curves with slope discontinuities at 28.8 ± 2.3, 30.5 ± 0.5, and 34.4 ± 0.7 °C. The slopes above T_c (−3.6 ± 0.5 K) were significantly less than those below (−7.7 ± 1.0 K; $p < 0.05$). The activity of the deoxycholate-treated enzyme was lower than that of the membrane-bound form and fitted best to a straight line.

Temperature Dependence of the Na^+/H^+ Antiporter. Antiporter activity was measured by using a 1.4 pH unit outwardly/directed proton gradient in three separate placental preparations. The proton flux in the absence of external sodium was subtracted from the sodium-stimulated rate to give the Na^+/H^+ activity. An Arrhenius plot of antiporter activity (one curve typical of three) is shown in Figure 4C. All the preparations showed biphasic curves with slope discontinuities at 26.6 ± 2.3, 27.2 ± 1.7, and 30.0 ± 0.3 °C. Slopes above T_c were significantly greater than the slopes below T_c ($p < 0.05$).

Discussion

Changes in the steady-state anisotropy of a fluorescent probe within a membrane may result from changes in the rotational rate of the probe (R), from alterations in the limiting anisotropy (r_∞; lipid packing order), from changes in probe lifetime, or from any combination of these (Lakowicz et al., 1979). Steady-state anisotropy data are therefore inadequate for a precise description of lipid structural characteristics or probe rotational motion. Nevertheless, steady-state anisotropy data can serve as a simple measure of membrane "fluidity" or motional restriction, especially for comparative purposes, using the large amount of data already accumulated for fluorophores such as DPH.

Although the values of steady-state anisotropy for DPH and TMA-DPH in placental microvillus vesicles are similar at lower temperatures (0.297 ± 0.007 and 0.311 ± 0.003 at 10 °C), due to immobilization of both probes in solid-phase lipid, there is a marked difference between the probes at 50 °C (0.204 ± 0.006 for DPH, 0.265 ± 0.012 for TMA-DPH). Large differences observed between DPH and TMA-DPH in synthetic lipid bilayers have been found to arise from the differing locations of the two fluorophores. TMA-DPH is anchored close to the bilayer surface by the charged trimethylamino group, probing the glycerol backbone/acyl chain region, while DPH is localized toward the hydrocarbon core of the bilayer (Engel & Prendergast, 1981a; Cranney et al., 1983). The difference between DPH and TMA-DPH anisotropy in MVV, like those in synthetic bilayers, becomes apparent at higher temperatures where the motion of TMA-DPH appears to be more limited than that of DPH.

The absolute steady-state anisotropy of DPH in placental brush border membranes is high relative to that reported for other epithelial brush border membranes. At 25 °C, r is 0.233 in rabbit renal brush border membrane vesicles (Verkman & Ives, 1986), 0.23 in bovine tracheal vesicles (Worman et al., 1986), and 0.239 in rat colonic brush border vesicles (Brasitus & Dudeja, 1985). The corresponding value for placental microvillus vesicles is 0.271 ± 0.005. The placental microvillus membrane would therefore appear to be more highly ordered than other brush border membranes which have been tested. It is not clear, however, whether corrections were made for vesicle emission scattering (by extrapolation to zero dilution) in the latter two reports cited; no correction was made in the former. It is possible that, with this correction, anisotropy values for the various brush border membranes might be similar.

The Arrhenius plots of the steady-state anisotropy of both DPH and TMA-DPH show biphasic curves with reproducible

breakpoints (T_c) at 26 °C, suggestive of a phase transition. Due to the composite nature of the steady-state anisotropy measurement, it is not possible to determine from these data alone whether the changes in steady-state anisotropy and the biphasic behavior result from changes in lipid packing, probe rotational rate, or probe lifetime with temperature. Anisotropy decay measurements showed increased rotational freedom (decreased r_∞) for both fluorophores with increasing temperature. When the model for an isotropic hindered rotator was used, DPH showed a biphasic decrease in r_∞ with temperature, with a breakpoint at 24 °C, characteristic of a lipid-phase transition, and similar to the temperature dependence of DPH steady-state anisotropy. TMA-DPH, however, demonstrates a monotonic decrease in r_∞ with increasing temperature, showing that while the rotational freedom of TMA-DPH increases with temperature this probe does not sense the phase transition reported by DPH at T_c. It is possible that the high cholesterol/phospholipid ratio (0.7/1) and sphingomyelin/phosphatidylcholine ratio (0.85/1) measured in this membrane (Smith & Brush, 1978; Kelley et al., 1979) may decrease order below and increase order above T_c in the region of the membrane closest to the lipid/water interface, potentially obscuring any transition that might be reported by TMA-DPH.

Although DPH and TMA-DPH have similar r_∞ values at 15 °C (DPH, 0.299 ± 0.002; TMA-DPH, 0.284 ± 0.007) due to solid-phase immobilization, increasing the temperature to 45 °C decreases DPH r ~2-fold more than TMA-DPH r_∞ (DPH, 0.192 ± 0.006; TMA-DPH, 0.256 ± 0.012; n = 3). These differences may also be due to the high cholesterol content of this membrane. The major effect of cholesterol on order in phosphatidylcholine vesicles, as measured by r_∞ for a series of anthroyloxy stearate and plamitate probes, was to increase r_∞ in the outer acyl chain area as compared to the bilayer core region (Kutchai et al., 1983). We can conclude from these data that increasing temperature decreases the lipid packing order in MVV, more so in the hydrophobic core of the membrane than toward the membrane surface. As part of this decrease in order, a solid to fluid, lipid-phase transition (as defined by r_∞) takes place at ~24 °C, although it is only observed by the probe in the hydrophobic core, not by the surface-anchored probe.

A number of reports have appeared in which an empirical relationship has been derived between r_∞ and r (Jahnig, 1979; Fulford & Peel, 1980; Van Blitterswijk et al., 1981). On the basis of these empirical equations, the r_∞ values for DPH calculated from our steady-state anisotropies were a poor fit to the values determined by anisotropy decay experiments. More importantly, if used with our TMA-DPH anisotropy values, these empirical relationships produced a spurious breakpoint in the temperature dependence of r_∞. The biphasic nature of the temperature dependence of TMA-DPH steady-state anisotropy resulted solely from the change in rotational rate with temperature which, over the full temperature range, was 0.179 ± 0.046 radian/ns, significantly greater than the change observed for DPH (0.109 ± 0.014 radian/ns). Therefore, use of these empirical relationships to derive r_∞ from r should be avoided and viewed as giving no information beyond that already contained in measurements of r. The almost linear plots of r_∞ against r for both DPH and TMA-DPH nevertheless emphasize that steady-state anisotropies are a measure of lipid packing order more than of probe rotational dynamics.

The fluorescence anisotropy decay measurements are predicated on the assumption that no ground-state heterogeneity exists for the fluorophore being measured. Measurements of DPH lifetimes both in SUV and in MVV demonstrated a single-lifetime component, unlike those of Barrow and Lentz (1985) or Parassassi et al. (1984). We did not find the ~3-ns lifetime component in our preparations which both the above reports concluded was a photolytic decomposition product and which may have obscured their analyses. It is possible, as pointed out by Barrow and Lentz (1985), that more than one component was present but that the ratio of the two lifetimes was less than 1.3, the limit of resolution with this type of instrumentation. A second short (<1 ns) component was present according to our analysis, at the level of 1–3%, well within the order of probable errors in the lifetime calculations (Barrow & Lentz, 1985) and possibly representing a small component of scattered light.

On the basis of the relatively homogeneous lifetimes for DPH and TMA-DPH, we used the formalism developed for a homogeneous isotropic hindered rotator to calculate R and r_∞. It is assumed that the rotational environment of the probe is also homogeneous, a commonly made assumption which is probably not valid for biological membranes in which lateral-phase separation may exist (see below). A modified approach, in which multifrequency tan Δ data are incorporated into the analysis, would help to resolve the rotational characteristics of a single fluorophore in heterogeneous environments (N. P. Illsley and A. S. Verkman, unpublished results).

The phase transition measured here by DPH r_∞ in MVV is broadened compared to the abrupt transitions observed for vesicles composed of a single phospholipid (Engel & Prendergast, 1981). Addition of cholesterol to artificial bilayers is known to cause such broadening (Presti, 1985). Another reason for phase transition broadening may be the coexistence of solid and fluid lipid phases whose proportions vary as the temperature is altered. This lateral-phase separation into solid and fluid domains has been observed in both synthetic and biological membranes [see Gordon & Mobley (1985) and Sklar (1984) for references]. DPH partitions equally between solid and fluid phases, and its fluorescence intensity is relatively insensitive to phase changes (Lentz et al., 1976). Barrow and Lentz (1985) examined domain behavior in pure dimyristoyl- or diplamitoylphosphatidylcholine vesicles but were only able to resolve solid- and fluid-phase components using extremely accurate measurements because of the insensitivity of DPH lifetime to the phase environment. In biological membranes using similar techniques, we observed apparent homogeneity of DPH lifetimes. In these circumstances, the parinaric acids have proven extremely useful probes, since the trans form partitions preferentially into solid-phase lipid and simultaneously undergoes a strong enhancement of fluorescence, whereas *cis*-parinaric acid partitions almost equally between solid and fluid phases (Sklar et al., 1979). More importantly, the lifetimes of the parinaric acids are extremely sensitive to their phase environment, displaying solid- and fluid-phase lifetimes which are more easily resolved than those of DPH (Wolber & Hudson, 1981). Blazyk et al. (1985) used the partitioning and enhancement properties of *t*-PnA to describe the solid to fluid transition in sarcoplasmic reticulum membranes by measuring changes in fluorescent intensity, but this method requires accurate measurement of quantum yield and temperature dependence of partitioning for quantitation of the lateral-phase separation.

Although ground-state lifetime heterogeneity was demonstrated for *t*-PnA and *c*-PnA in MVV, the temperature dependence of r for these probes provides a qualitative measure of lipid order through the phase transition. The steady-state

Table II: Temperature Dependence Breakpoints for Placental Microvillus Membrane Functions[a]

membrane function	breakpoint (°C)	ref
fluorescence rotational studies		
steady-state anisotropy, DPH	26 ± 2	
steady-state anisotropy, TMA-DPH	26 ± 3	
DPH limiting anisotropy	24 ± 2	
fluorescence lifetime studies		
c-PnA α_1 midpoint component	27	
membrane-associated enzymes		
alkaline phosphatase	28 ± 1	
aminopeptidase M	31 ± 3	
membrane transport		
Na^+/H^+ exchange	28 ± 2	
water transport	27 ± 3	(a)
urea transport	27 ± 2	(b)
glucose transport	24	(c)
proton transport	ND[b]	(d)

[a] All values taken from present report except for (a) Illsley & Verkman (1986a), (b) Illsley & Verkman (1986b), and (c) Ingermann & Bissonnette (1983), and (d) Cabrini et al. (1986). [b] ND, not detected.

anisotropies suggest that both *c*-PnA and *t*-PnA move from a more to a less highly ordered environment with increasing temperature but that *t*-PnA exists in a more highly ordered environment than *c*-PnA particularly at lower temperatures as predicted by the preferential partitioning of *t*-PnA into solid-phase domains.

The conclusions drawn from the steady-state anisotropy data were confirmed by the quantitative assessment of phase behavior determined from the lifetime heterogeneity analyses of parinaric acid fluorescence. The solid-phase lifetimes for both *t*-PnA and *c*-PnA were 4–5-fold higher than the fluid-phase lifetimes at all temperatures. The existence of two well-resolved lifetimes representing solid and fluid lipid phases provided an excellent method of assessing the contributions of the two phases to the membrane structure over a wide temperature range. At lower temperatures, more than 80% of the membrane was composed of a solid lipid phase, while at high temperatures this dropped to less than 15%. While both probes showed similar phase composition at the extremes of temperature, *c*-PnA displayed a shift to the fluid phase at a lower temperature than did *t*-PnA, consistent with the partition behavior described by previous reports (Wolber & Hudson, 1981; Schroeder, 1983). The half-point of the transition for *c*-PnA was ~27 °C, very similar to T_c determined from r and r_∞ measurements, suggesting that the solid/fluid partition ratio is close to 1.0, similar to that reported by Schroeder (1983) for rat liver plasma membranes (0.92), but larger than that reported for synthetic phosphatidylcholine mixtures (0.6) by Sklar et al. (1979).

The lifetime data demonstrated that solid and fluid phases coexist over a wide temperature range in a natural membrane. The phase transition results from temperature-related changes in the solid/fluid composition of the membrane. An interesting question which arises from this analysis is the location and nature of the ~20% of lipid which appears to be in fluid form below T_c and the 10–15% of lipid which appears to remain in solid form above T_c. The lipid which remains in a fluid state below T_c may be composed in part of the annular ring of lipid which surrounds membrane protein and which is "fluid-like" in its behavior (Kimmelman et al., 1979).

We investigated the temperature dependences of a number of membrane-bound proteins to discover whether the lipid-phase transition observed by DPH r_∞ and *c*-PnA/*t*-PnA fluorescence lifetimes affected their function. Alkaline phosphatase and aminopeptidase M are enzymes whose activities are accessible only on the external surface of the microvillus membrane and do not require an intact, sealed membrane for observation of their function. The assays used were single-step cleavage assays, avoiding the problems of linked-assay temperature dependences. The sodium/proton antiporter is an integral membrane protein which requires that vesicles be intact in order to observe activity. All three proteins showed breaks in their temperature dependence curves in the region of the previously determined phase transition. The Arrhenius plots of alkaline phosphatase and aminopeptidase activities were linear after membrane solubilization, demonstrating that the breakpoint in the plot for these membrane-bound enzymes was caused by the membrane phospholipids and was not an intrinsic effect. We conclude from these data that the membrane phase transition can influence the catalytic or transport properties of membrane-bound proteins.

There is additional evidence that the lipid-phase transition has widespread effects on membrane functions, as summarized in Table II. Water and urea transport, transport functions which are in part lipid mediated, showed discontinuities in their activation energies at the phase transition temperature (Illsley & Verkman, 1986a,b). A similar biphasic temperature dependence has been shown for glucose transport, a passive, sodium-independent carrier-mediated process similar to that observed in the erythrocyte (Johnson & Smith, 1980). Interestingly, of all MVV enzyme and transport functions studied, only the passive proton permeability has a constant activation energy at all temperatures (Cabrini et al., 1986).

Registry No. Alkaline phosphatase, 9001-78-9; aminopeptidase M, 9054-63-1.

REFERENCES

Barrow, D. A., & Lentz, B. R. (1983) *J. Biochem. Biophys. Methods 7*, 217–234.

Barrow, D. A., & Lentz, B. R. (1985) *Biophys. J. 48*, 221–234.

Bartlett, G. R. (1959) *J. Biol. Chem. 234*, 466–468.

Bevington, P. R. (1969) *Data Reduction and Error Analysis for the Physical Sciences*, McGraw-Hill, New York.

Blazyk, J., Wu, C.-J., & Wu, S.-C. (1985) *J. Biol. Chem. 260*, 4845–4849.

Bligh, E. G., & Dyer, W. J. (1959) *Can. J. Biochem. Physiol. 37*, 911–918.

Brasitus, T. A., & Dudeja, P. K. (1985) *Biochim. Biophys. Acta 819*, 10–17.

Cabrini, G., Illsley, N. P., Verkman, A. S. (1986) *Biochemistry 25*, 6300–6305.

Cranney, M., Cundall, R. B., Jones, G. R., Richards, J. T., & Thomas, E. W. (1983) *Biochim. Biophys. Acta 735*, 418–425.

Engel, L. W., & Prendergast, F. G. (1981) *Biochemistry 20*, 7338–7345.

Fulford, A. J. C., & Peel, W. E. (1980) *Biochim. Biophys. Acta 598*, 237–245.

George, S. G., & Kenny, A. J. (1973) *Biochem. J. 134*, 43–57.

Gordon, L. M., & Mobley, P. W. (1985) in *Membrane Fluidity in Biology* (Aloia, R. C., & Boggs, J. M., Eds.) Vol. 4, pp 1–49, Academic Press, Orlando, FL.

Houslay, M. D., Dipple, I., Rawal, S., Sauerheber, R. D., Esgate, J. A., & Gordon, L. M. (1980) *Biochem. J. 190*, 131–137.

Illsley, N. P., & Verkman, A. S. (1986a) *J. Membr. Biol.* (in press).

Illsley, N. P., & Verkman, A. S. (1986b) *Placenta 7*, 481.

Ingermann, R. I., & Bissonnette, J. M. (1983) *Biochim. Biophys. Acta 734*, 329–335.

Ives, H. E., & Verkman, A. S. (1985) *Am. J. Physiol. 249*, F933–F940.

Jahnig, F. (1979) *Proc. Natl. Acad. Sci. U.S.A. 76*, 6361-6365.
Johnson, L. W., & Smith, C. H. (1980) *Am. J. Physiol. 238*, C160-C168.
Kelley, L. K., King, B. F., Johnson, L. W., & Smith, C. H. (1979) *Exp. Cell Res. 123*, 167-176.
Kimmelman, D., Tecoma, E. S., Wolber, P. K., Hudson, B. S., Wickner, W. T., & Simoni, R. D. (1979) *Biochemistry 18*, 5874-5880.
Kutchai, H., Chandler, L. H., & Geddis, L. M. (1980) *Biochim. Biophys. Acta 600*, 870-881.
Kutchai, H., Chandler, L. H., & Zavoico, G. B. (1983) *Biochim. Biophys. Acta 736*, 137-149.
Lakowicz, J. R., Prendergast, F. G., & Hogen, D. (1979) *Biochemistry 18*, 508-519.
Lakowicz, J. R., Cherek, H., & Balter, A. (1981) *J. Biochem. Biophys. Methods 5*, 131-146.
Lentz, B. R., Barenholz, Y., & Thompson, T. E. (1976) *Biochemistry 15*, 4521-4528.
Lentz, B. R., Moore, B. M., & Barrow, D. A. (1979) *Biophys. J. 25*, 489-494.
Livingstone, C. J., & Schachter, D. (1980) *J. Biol. Chem. 255*, 10902-10908.
Lowry, O. H., Rosebrough, N. J., Farr, A. L., & Randall, R. J. (1951) *J. Biol. Chem. 193*, 265-275.
Parasassi, T., Conti, F., Glaser, M., & Gratton, E. (1984) *J. Biol. Chem. 259*, 14011-14017.
Prendergast, F. G., Haugland, R. P., & Callahan, P. J. (1981) *Biochemistry 20*, 7333-7338.
Presti, F. T. (1985) in *Membrane Fluidity in Biology* (Aloia, R. C., & Boggs, J. M., Eds.) Vol. 4, pp 97-146, Academic Press, Orlando, FL.
Schroeder, F. (1983) *Eur. J. Biochem. 132*, 509-516.
Silvius, J. R., Read, B. D., & McElhaney, R. N. (1978) *Science (Washington, D.C.) 199*, 902-904.
Sklar, L. A. (1984) *Biomembranes 12*, 99-131.
Sklar, L. A., Miljanich, G. P., & Dratz, E. A. (1979) *Biochemistry 18*, 1707-1716.
Smith, N. C. & Brush, M. G. (1978) *Med. Biol. 56*, 272-276.
Spencer, R. D., & Weber, G. (1969) *Ann. N.Y. Acad. Sci. 158*, 361-376.
Teale, F. W. J. (1969) *Photochem. Photobiol. 10*, 363-374.
Van Blitterswijk, W. J., Van Hoeven, R. P., & Van der Meer, B. W. (1981) *Biochim. Biophys. Acta 644*, 323-332.
Verkman, A. S., & Ives, H. E. (1986) *Am. J. Physiol. 250*, F633-F643.
Weber, G. (1977) *J. Chem. Phys. 66*, 4081-4091.
Weber, G. (1981) *J. Phys. Chem. 85*, 949-953.
Wolber, P. K., & Hudson, B. S. (1981) *Biochemistry 20*, 2800-2810.
Worman, H. J., Brasitus, T. A., Dudeja, P. K., Fozzard, H. A., & Field, M. (1986) *Biochemistry 25*, 1549-1555.
Yuli, I., Wilbrandt, W., & Shinitzky, M. (1981) *Biochemistry 20*, 4250-4256.

Isolation and Characterization of Nucleoprotein Assembly Intermediates of Tobacco Mosaic Virus†

Walter Godchaux, III, and Todd M. Schuster*
Department of Molecular and Cell Biology, The University of Connecticut, Storrs, Connecticut 06268
Received July 9, 1986; Revised Manuscript Received October 2, 1986

ABSTRACT: During assembly of tobacco mosaic virus from pure RNA and 20S capsid protein aggregates under conditions where protein is limiting, partially assembled intermediates of specific sizes accumulate; these were isolated on sucrose density gradients. The earliest intermediate found in substantial quantity sedimented at 56 S and was shown, by measurement of its buoyant density and of the length of the RNA segment protected by the capsid protein from nuclease digestion, to consist of RNA that is 13% encapsidated (corresponding to a rod length of about 39 nm); the next intermediate sediments at 78 S and is 18% encapsidated (corresponding to a rod length of about 54 nm). Studies of the distribution of intermediates at various input ratios of protein/RNA indicated that their accumulation results from decreases in the rate constants for protein binding that are local to specific points in the course of encapsidation. After extensive nuclease digestion, the RNA still associated with the first intermediate was shown to include a portion that is unencapsidated. This segment of the RNA may be a region of stable secondary structure that confers the nuclease resistance despite the lack of protection by capsid protein. Such RNA secondary structure, if it exists, would also cause the accumulation of intermediates by imposing an energy barrier to subsequent rod elongation.

Since Fraenkel-Conrat and Williams (1955) first demonstrated the cell-free self-assembly of tobacco mosaic virus (TMV)[1] from its constituent single strand of RNA and subunits of its single coat protein (TMVP), there has been considerable interest in both the structural and mechanistic details of the protein-RNA and protein-protein interactions. Extensive solution studies have revealed details of some aspects of the kinetics (Schuster et al., 1979; Shire et al., 1979; Fukuda et al., 1978; Schuster & Scheele, 1974) and mechanism of the self-association of the coat protein, in the absence of RNA, to form cylindrical disk aggregates and viruslike, helical rods

† This research was supported by a grant from the National Institutes of Health (AI11573).

[1] Abbreviations: TMV, tobacco mosaic virus; TMVP, TMV coat protein; PAR, partially assembled rod; BMV, brome mosaic virus; EGTA, ethylene glycol bis(β-aminoethyl ether)-*N,N,N',N'*-tetraacetic acid; kb, kilobase(s).

0006-2960/87/0426-0454$01.50/0